Journal of Agricultural Science; Vol. 11, No. 11; 2019
ISSN 1916-9752 E-ISSN 1916-9760
Published by Canadian Center of Science and Education

Aboveground Biomass Estimates of *Araucaria angustifolia* (Bertol.) Kuntze, Using Vegetation Indexes in Wolrdview-2 Image

Luiz Carlos Pietrowski Basso[1], Vagner Alex Pesck[1], Mailson Roik[2], Afonso Figueiredo Filho[1], Thiago Floriani Stepka[3], Gerson dos Santos Lisboa[4], Ismael Konkol[1], André Felipe Hess[3] & Ana Paula Brandalize[1]

[1] Department of Forest Engineering, Central Western Parana State University, Irati, Paraná, Brazil

[2] Federal University of Parana, Curitiba, Paraná, Brazil

[3] Department of Forest Engineering, Santa Catarina State University, Lages, Santa Catarina, Brazil

[3] Center for Training in Technosciences and Innovation, Federal University of Southern Bahia, Itabuna, Bahia, Brazil

Correspondence: Vagner Alex Pesck, Department of Forest Engineering, Central Western Parana State University, PR 153-Km 7-Neighborhood Riozinho. Pillar Box 21, Irati, Paraná, Brazil. Tel: 55-423-421-3095. E-mail: vapesck@unicentro.br

Received: April 9, 2019 Accepted: May 15, 2019 Online Published: July 31, 2019

doi:10.5539/jas.v11n11p93 URL: https://doi.org/10.5539/jas.v11n11p93

Abstract

The present research aims to evaluate the biomass estimates of *Araucaria angustifolia* (Bertol.) Kuntze trees obtained by the direct method, then present results generated from a 2.0 m resolution spectral image Worldview-2 satellite. The quantification of the biomass in the field was first carried out of 29 trees of the specie of interest with DBH ≥ 40 cm and then with the image aid the crowns were delimited for analysis. From the spectral bands (B2-blue, B3-green, B4-yellow, B5-red, B6-near red, B7-near infrared 2 and B8-near infrared 2), it was possible to obtain vegetation indexes proposed by the literature (NDVI, NDVI_2, RS and SAVI_0,25) and later incorporated with dendrometric data a correlation matrix was formed. Additionally, mathematical equations were used to estimate biomass and carbon as a function of dendrometric variables and information obtained from the satellite image processing. From these equations, the ones that presented better results were those that contained independent dendrometric variables (DBH) and those that contained vegetation indices (NDVI_2 and NDVI). For the dendrometers, the relative error found was 14.42% and 14.32% for biomass and carbon respectively, while for the digital ones, NDVI_2 found a relative error of 37.82% and an adjusted coefficient of determination of 0.88 in the biomass equations. In the carbon equations, the NDVI variable presented the best results, being 38.56% the relative error and 0.87 the determination coefficient.

Keywords: forest Inventory, regression, remote sensing

1. Introduction

Over the last few years there has been increasing interest in using remote sensing data to provide efficient estimates of aboveground biomass (AGB) and carbon because they are able to collect repetitive and comprehensive observations from local to global scales (Avitabile et al., 1998; Batistella, 2005; Lu et al., 2004; Sarker & Nichol, 2011; Soenen et al., 2010; Dong et al., 2012). The AGB cannot be measured directly from air or space, so the approaches using remote sensors are developed by linking information derived from remote sensing data and measured biomass values in the field (Zhu & Liu, 2015). The close association between tree height, DBH and wood volume models have a high explanatory power for forest biomass estimates (Koch, 2010).

Forest biomass is one of the main resources for an emerging sustainable bioeconomy (Becker et al., 2009). Therefore, sustainable management of forest ecosystems as well as climate protection as mechanisms for Reducing Emissions from Deforestation and Degradation (REDD+) depend on reliable and concise information on the spatial and temporal distribution of forest biomass (Maack et al., 2015). In addition, precise estimates are needed to assess the ecosystem services potential (eg erosion control). In the remote sensing area, several sensors and approaches were evaluated to model above-ground biomass (Lu, 2006; Anaya et al., 2009; Koch, 2010;

Clark et al., 2011; Maack et al., 2015). Most frequent surveys have used remote sensing predictors in combination with field measurements to train parametric or non-parametric regression models (Fassnacht et al., 2014).

The biomass estimation using high-resolution spatial images, such as the Worldview-2 sensor, has been extensively studied with accurate experimental results (Dube et al., 2014; Mutanga et al., 2012; Robinson et al., 2016; Sibanda et al., 2015). However, the operational use of this data in automated procedures to be applied to forest inventories and large-scale forest management is still limited to a small number of cases (Fassnacht et al., 2017).

More precisely, the 8-band Worldview-2 multispectral sensor is characterized by a better spatial resolution of 2 m and two new spectral bands with unique band configurations such as red-edge (705-745 nm) and near infrared 2 (860-1040 nm) when compared to other multispectral sensors. Due to these unique advances, vegetation indexes as the Normalized Difference Vegetation Index (NDVI), Simple Reason (SR), SAVI (Soil Adjusted Vegetation Index), EVI (Enhanced Vegetation Index), calculated from the WordView-2 data are more sensitive to subtle variations in the biochemical/physical properties of the plant and could, therefore, improve the quantification and mapping of BIAS and carbon in densely forested areas such as the Araucaria forests.

The literature demonstrates that vegetation indexes derived from Worldview-2 are effective in characterizing forest biomass and other biophysical characteristics of vegetation and many which are sensitive to reflectance in the visible and near-infrared portions of the electromagnetic spectrum (Adam et al., 2014; Dube et al., 2014; Mutanga et al., 2012; Robinson et al., 2016). Beyond, sensors with few, but important spectral bands (*i.e.*, the red band) are critical to minimize any redundancy and unnecessary noise associated with hyperspectral images. Due to these unique sensor characteristics the introduction of new generation multispectral sensors is in this study, verifying the usefulness in the carbon standards monitoring stored in terrestrial ecosystems on landscape scale with high precision and accuracy.

Therefore, the objective of this work was to estimate the aerial biomass and organic carbon of native trees of *Araucaria angustifolia* (Bertol.) Kuntze in an Araucaria Forest fragment using vegetation indexes in Wolrdview-2 image.

2. Method

2.1 Characterization of the Study Area

This research was developed in a fragment of Araucaria forest (IBGE, 1992) located in the subbasin of the Imbituvão river, Assungui community, municipality of Fernandes Pinheiro, State of Parana. The municipality is located in the Center-South region of Parana (25º27′ S and 50º35′ W), at an altitude of 893 meters (Wrege et al., 2012). The rural property where the fragment is inserted has a total area of 47.9 hectares, of which 24.5 hectares are forest remnants (Figure 1), that comprise part of the studies of the Imbituvão Project developed by the Forestry Engineering Department of Central Western Parana State University (UNICENTRO).

According to Koppen classification, the climate region is characterized as Subtropical Moist Mesothermal (Cfb), that means, it has fresh summers and winters with the occurrence of severe frost and that hardly has dry seasons. The average annual temperature is 18 °C, with a minimum temperature of -2 °C and maximum of 32 °C (Simepar, 2012).

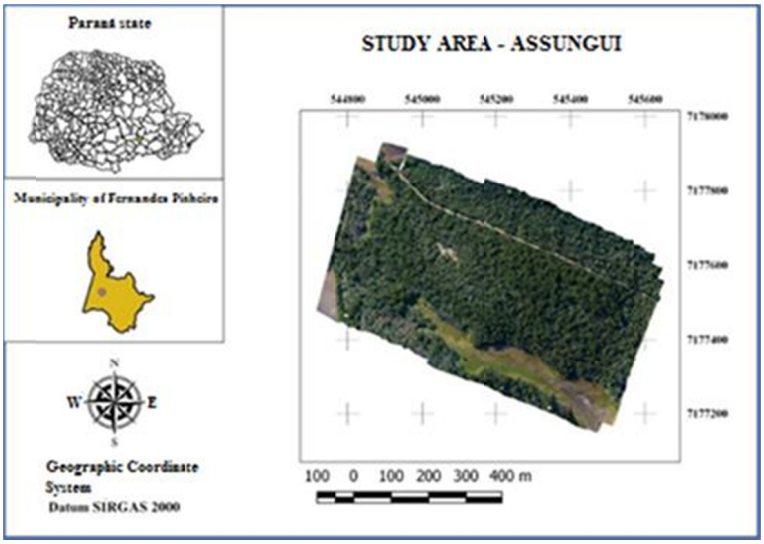

Figure 1. Location of the study area in municipality of Fernandes Pinheiro, State of Parana, Brazil

2.2 Determination of Biomass by Direct Method

The determination of the biomass in the field was performed according to the direct method of quantification, by sampling 29 trees with diameter at breast height (DBH) ≥ 40 cm, randomly distributed in the fragment, aiming to contemplate the diametric variability (Table 1).

After the trees were felled, the following components were separated: leaves, branchs and stem. Each component was weighed separately to obtain the green biomass. After that, samples of each component were collected.

The samples were taken to the laboratory and dried in an air circulation greenhouse and at a temperature of 65 °C until reaching constant weight for further determining the moisture content and preparation for chemical analysis of the organic carbon content.

In order to determine the carbon content, the samples were first fragmented using a planing saw, crushed in a Willey and Croton mill with a 20 mesh sieve and then analyzed by the direct combustion method using a C-144 LECO elemental analyzer. In this method, the sample is placed in a pure oxygen environment with a temperature typically set at 1350 °C and is then subjected to complete combustion, releasing the carbon as carbon dioxide, which is measured by infrared sensors. The instrument converts the result to a percentage using a predefined equation in the software that takes into account sample weight, calibration, and known moisture value (LECO, 2008). After determining the organic carbon content in each sampled fraction, it was then multiplied by the dry biomass, thereby obtaining the amount of organic carbon per component. The detail methodology is described in Roik (2018).

Table 1. Volume, age and number of individuals sampled from the specie *Araucaria angustifolia* (Bertol.) Kuntze

Variable	Variation	DBH Class (cm)			Total
		40-50	50-60	60-70	
Trees sampled	Male	3	7	3	13
	Female	9	6	1	16
	Total	12	13	4	29
Volume (m^3 $tree^{-1}$)	Minimum	1.37	2.34	3.89	1.37
	Average	1.99	3.31	4.64	2.94
	Maximum	2.74	4.32	5.30	5.30
Age (years)	Minimum	80	87	99	80
	Average	99	101	126	104
	Maximum	111	119	188	188

The determination of the age of the trees was made by counting the growth rings of the disc taken from the base of each tree sampled.

2.3 Obtaining and Preprocessing the Worldview-2 Image

For the biomass estimate through remote sensing, a multispectral image with spatial resolution of 2.0 meters was used. The image containing a scene from the study area (Figure 2) was obtained on December 21, 2012. The spectral resolution of the WorldView 2 image can be seen in Table 2.

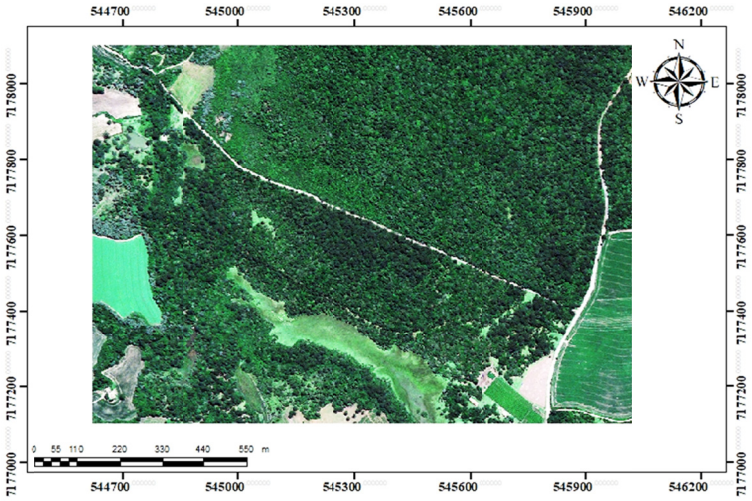

Figure 2. WorldView-2 image of the study area in the RGB composition (R5G3B2)

Table 2. Spectral resolutions of the worldview 2 satellite bands

Spectral Band	Minimum (nm)	Maximum (nm)	Amplitude (nm)	Average (nm)
B&W	450	800	350	625
B1(Costal)	400	450	50	425
B2(Blue)	450	510	60	480
B3(Green)	510	580	70	545
B4(Yellow)	585	625	40	605
B5(Red)	630	690	60	660
B6(Near Red)	705	745	40	725
B7(Near Infrared 1)	770	895	125	832
B8(Near Infrared 2)	860	1040	180	950

2.4 Atmospheric Correction and Digital Numbers Conversion Into Radiance/Reflectance

For estimating aerial biomass and organic carbon by remote sensing, it is necessary to establish quantitative relations between the digital numbers (DN's) of the image and parameters of the target object. Thus, the conversion of DN to reflectance should be performed, in order to minimize the illumination conditions variation in the spectral behavior of the target (Chuvieco, 1990).

According to Chuvieco (1990) and Watzlawick et al. (2009), the conversion process is portrayed in three phases: (1) DN's conversion to radiance values; (2) radiance values conversion to reflectance values; (3) atmospheric correction of the image, necessary, since the presence of elements in the atmosphere as aerosols and water vapors make the energy that comes from the sun to be dispersed before reaching the target object.

For the process of converting image DN's into apparent two-way radiance, Equation 1 was used.

$$L\lambda\ \text{Pixel, Band} = \frac{\mathbf{K}\ \text{Band} \times \mathbf{q}\text{Pixel, Band}}{\mathbf{\Delta\lambda}\ \text{Band}} \quad (1)$$

Where, Lλ Pixel, Band = Pixel spectral radiance ($W\text{-}m^{-2}\text{-}sr^{-1}\text{-}\mu m^{-1}$); KBand = Absolute radiometric calibration factor of a particular band ($W\text{-}m^{-2}\text{-}sr^{-1}\text{-}count^{-1}$); qPixel, Band = Pixel's DN of the corrected radiometric image

(count); Δλ Band = Effective bandwidth (μm) of a band. The calibration factor and the effective bandwidth are available in the image file metadata.

For the apparent bidirectional radiance values conversion to apparent bidirectional reflectance, Equation 2 was used.

$$\rho\lambda \text{ Pixel, Band} = \frac{L\lambda \text{ Pixel, Band} \times d\ TS^2 \cdot \pi}{Esun\ \lambda Band \times \cos(\Theta s)} \quad (2)$$

Where, ρλ Pixel, Band = Apparent bidirectional reflectance; Lλ Pixel, Band = Apparent two-way radiance; d TS = Earth-Sun Distance; π = 3.141592; Esun λBand = Sun average irradiance at the top of the atmosphere for each band; cos(Θs) = zenith solar angle.

The image atmospheric correction was performed in the FLAASH module, which uses MODTRAN4 (Moderate Resolution Atmospheric and Transmittance Model) radiative transfer code. This code processes data from hyperspectral and multispectral sensors in the short-wave infrared (SWIR), visible and ultraviolet (UV) bands, thus minimizing the effects of scattering and atmospheric absorption. In addition to performing the correction for the pixel mix due to surface scattering, the code also calculates the average scene visibility (aerosol/mist). The FLAASH method can also be used to correct images collected in vertical or inclined geometries (Silva et al., 2017).

2.5 Generation of Vegetation Indices

The vegetation indexes analyzed were:

a) Simple Reason (SR): where (Cohen et al., 1992) suggests being the first true index among all others. It's expressed by the ratio between the near infrared band 1 and the red band, whose relevant characteristic is to provide information on vegetation biomass (Schlerf et al., 2005). Its expression (3) is defined as:

$$R = \frac{B7_{nir1}}{B5_{red}} \quad (3)$$

Where, B7 is the Near Infrared 1 band and B5 is the red band.

b) NDVI (Normalized Difference Vegetation Index): proposed by Gurgel (2003), the index starts from the principle of the difference between the measurement of the reflectance in the near infrared channels and the red one by the sum of the same channels, that is, using the SR bands (4):

$$NDVI = \frac{B7_{nir1} - B5_{red}}{B7_{nir1} + B5_{red}} \quad (4)$$

From the NDVI (5, 6, 7), some tests were performed in this work, altering some bands, and thus three new indices were tested:

$$NDVI\ (1) = \frac{B8_{nir2} - B5_{red}}{B8_{nir2} + B5_{red}} \quad (5)$$

$$NDVI\ (2) = \frac{B7_{nir1} - B6_{red\text{-}edge}}{B7_{nir1} + B6_{red\text{-}edge}} \quad (6)$$

$$NDVI\ (3) = \frac{B8_{nir2} - B6_{rededge}}{B8_{nir2} + B6_{rededge}} \quad (7)$$

Where, B8 is the band of Near Infrared 2and B6 is the band of the Near Red.

c) SAVI (Soil Adjusted Vegetation Index): one of the most recurrent problems in the estimation of vegetation indexes in satellite images is the influence that the soil exerts on the characterization of the plants canopy and Huete (1988) thinking about that formulated the SAVI, which tries to minimize the influence exerted from a factor (L), aggregated in the expression, which can be: 1.0, when it is a very low coverage, 0.5 for covers considered intermediate and 0.25 for those of high density. In this research two factors (0.25 and 0.5) were tested, whose expression was described as (8):

$$SAVI = \frac{(1 + L) \times (B7_{nir1} - B5_{red})}{(L + B7_{nir1} + B5_{red})} \times (1 + L) \quad (8)$$

2.6 Sampling of Spectral Variables and Adjustment of the Mathematical Model

For obtaining the digital variables, initially a buffer was generated, considering the crown diameters of the sampled trees, through their (x, y) coordinates. Subsequently, the image clipping was performed and thus the mean values of the pixels of each tree sampled were extracted. This step was performed for all indexes under analysis as well as for each spectral band separately. Figure 3 illustrates how were arranged the delimitations made in the image for the calculations of each tree.

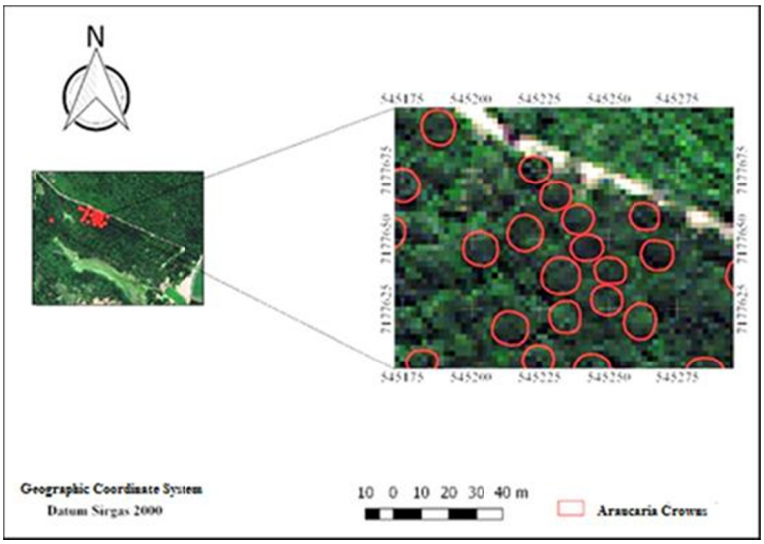

Figure 3. Araucaria crowns delimitation

2.7 Statistical Analysis

Statistical analysis of the data was performed based on the correlation between aerial biomass and organic carbon data with the digital data, which correspond to the image values (reflectance of the spectral bands B2 to B8 and reflectance of the vegetation indices SR, NADVI, NDVI (1, 2, 3) and SAVI).

For the estimation of aerial biomass and organic carbon (dependent variables), the equations were generated by the Stepwise procedure, considering the reflectance values of spectral bands and vegetation indexes as independent variables. The evaluation of the equations was done based on the higher adjusted determination coefficient (R^2 adj), lower standard error of estimate (%) and analysis of the residuals distribution.

3. Results and Discussion

3.1 Images of the Vegetation Indexes Generated From the Spectral Bands

The application of the vegetation indexes as well as the reflectance of the Near Infrared spectral band in the study area resulted in thematic maps, which are presented in Figure 4.

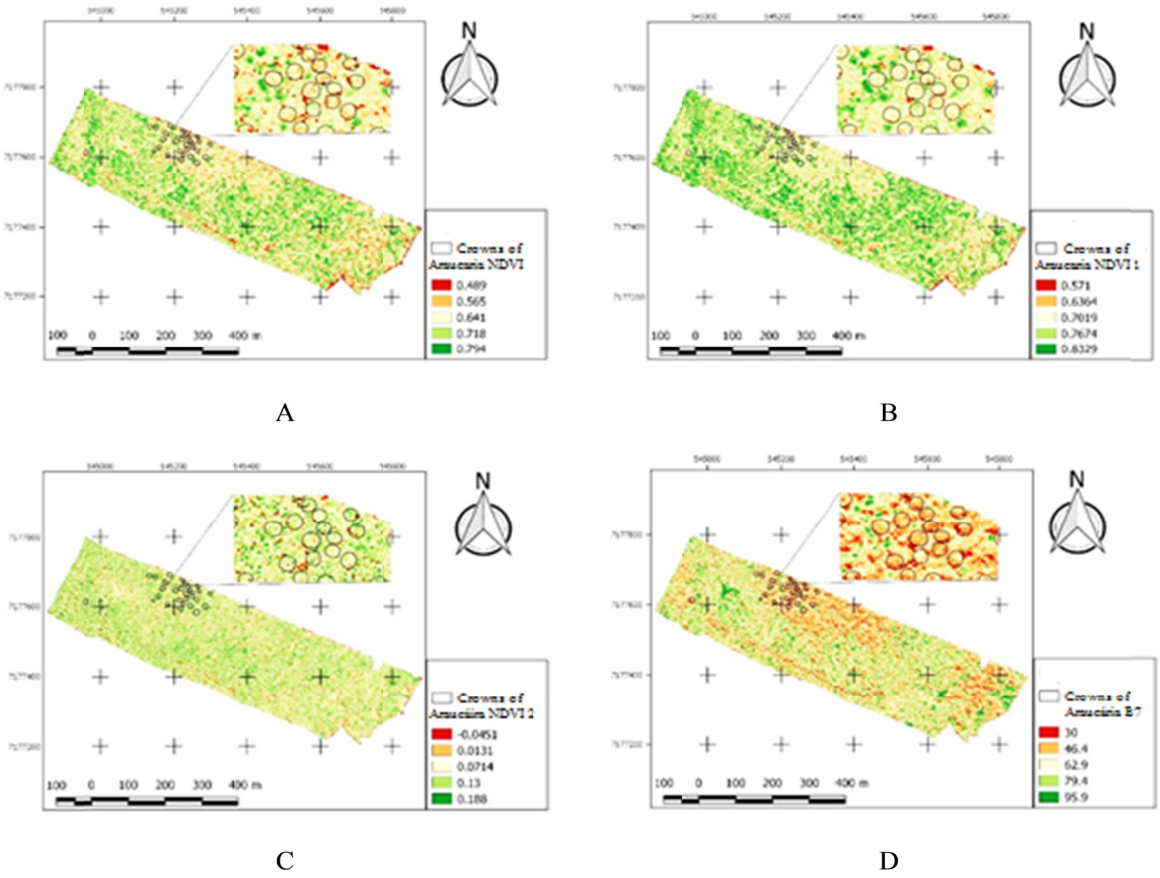

Figure 4. Study area thematic maps obtained based on: (A) Vegetation Index NDVI; (B) Vegetation Index NDVI_1; (C) Vegetation Index NDVI_2 and (D) Spectral Band B7-Near Infrared

The classes that correspond to the lowest values of the evaluated indexes correspond to the *Araucaria angustifolia* and shade regions. According to Watzlawick et al. (2009), coniferous forests have a lower spectral response in the near infrared region when compared to deciduous forests.

As the class values increase, other objects become more evident in the scene, thus gaining greater prominence due to spectral response. The classes can be understood as exposed soil, grasses and the own vegetation corresponding to the leafy species, expressing the highest reflectance values.

When performing the visual interpretive analysis of the generated thematic maps, no difference was observed regarding the spectral responses of the objects in the scenes generated by NDVI and NDVI_1 (Figure 6A and 6B, respectively). On the other hand, in the scene obtained by NDVI_2 (Figure 6C) the differences become more evident. The results of the research by Adam et al. (2014) have demonstrated that the utility of EVI and NDVI vegetation indices calculated from hyperspectral images in the estimation of biomass in dense forests is a challenging task with broadband satellite sensors because of the proximity of the spectral responses of the objects.

Sarker and Nichol (2011) stated that the performance in the biomass estimation can be significantly increased using texture parameters using high resolution optical sensors such as the AVNIR-2 sensor of the ALOS platform. However, obtaining these data sets, that is hyperspectral, LIDAR and radar, remains a major challenge, especially in developing countries. In addition to these data sets, the limited space/coverage area is associated with high costs/data volume, as well as high pre-processing costs compared to Worldview-2. Therefore, it is prudent to examine the potential of integrating high resolution multispectral sensors and environmental variables in the quantification and mapping of biomass and carbon.

3.2 Statistical Analysis

The correlation matrix generated from the biomass and carbon data and the Worldview-2 digital image data, such as vegetation indexes and spectral bands, are presented in Table 3.

Table 3. Correlation matrix between obtained data in the field and digital values of the indexes and spectral bands

	DBH	DW	Carb	NDVI	NDVI_1	NDVI_2	NDVI_3	SR	SAVI	B1	B7
DBH	1.00	0.93	0.93	-0.06	-0.12	0.13	-0.03	-0.06	-0.06	-0.10	-0.20
DW	0.93	1.00	1.00	0.02	-0.06	0.22	0.03	-0.01	0.01	-0.10	-0.11
Carb	0.93	1.00	1.00	0.01	-0.06	0.22	0.03	-0.01	0.01	-0.10	-0.10
NDVI	-0.06	0.02	0.01	1.00	0.96	0.58	0.52	0.98	1.00	0.11	0.14
NDVI_1	-0.12	-0.06	-0.06	0.96	1.00	0.49	0.63	0.97	0.96	0.07	0.03
NDVI_2	0.13	0.22	0.22	0.58	0.49	1.00	0.75	0.53	0.58	-0.13	0.04
NDVI_3	-0.03	0.03	0.03	0.52	0.63	0.75	1.00	0.54	0.51	-0.17	-0.19
SR	-0.06	-0.01	-0.01	0.98	0.97	0.53	0.54	1.00	0.98	0.09	0.05
B1	-0.10	-0.10	-0.10	0.11	0.07	-0.13	-0.17	0.09	0.11	1.00	0.79
B7	-0.20	-0.11	-0.10	0.14	0.03	0.04	-0.19	0.05	0.15	0.79	1.00

Note. DBH = diameter at breast height (cm); DW = Dry weight (kg); Carb = Carbon (kg); NDVI = Normalized Difference Vegetation Index; NDVI (2 and 3) = Vegetation Index using the *red-edge* band; SR = Simple Reason; SAVI = Soil Adjusted Vegetation Index; B1 = Spectral Band Costal Blue and B7 = Near Infrared Spectral Band.

The biomass and carbon correlations, presented statistical significance (p value = 0.000) in relation to DBH. This result can also be seen in the research of Watzlawick et al. (2009) who also worked with the same variables.

When the data (biomass and carbon) are compared with the image data, which correspond to vegetation indexes and spectral bands, they are not statistically significant (p value > 0.05). However, index NDVI_2 has the largest positive correlation in relation to biomass and carbon, 0.223 and 0.222, respectively. These values can be explained by the fact that the bands that integrate the index are the near infrared 1 and the red-edge band, which in turn have a very strong relation with spectral behavior of the plant.

Therefore, the presence of single and strategically positioned bands, such as red-edge and near-infrared bands, has the potential to improve the accuracy of biomass and carbon estimates of vegetation when compared to other sensors, strengthening vegetation mapping performance (Dube et al., 2014; Mutanga et al., 2012; Ozdemir e Karnieli, 2011; Robinson et al., 2016; Sibanda et al., 2015a; Tan et al., 2003). For example, Robinson et al. (2016), found with red-edge and near infrared double bands (NIR1 and NIR2) the best combination for species discrimination. Table 4 shows equations adjusted from the regression using the Stepwise method.

In the study of biomass (Table 4) there was a minimum difference in relation to the adjusted determination coefficient (R^2 adj) of each equation. Equation (2) stands out showing the highest value of R^2 adj (0.87), but with the standard error (Syx%), there is a notable disparity between the four proposed models, especially those involving only the vegetation indexes. Equation 1 presents the lowest standard error (14.42%), because considers only the variable DBH (cm), which is directly related to biomass and carbon. However, Equation 2, which uses the *red-edge* and near infrared band 1, obtained a standard error of 37.82%, and R^2adj of 0.87.

Table 4. Equations to estimate the aerial biomass and organic carbon of *Araucaria angustifolia* obtained by the Stepwise procedure

R.M.	Model	Syx%	R^2adj	β_0	β_1	β_2	β_3	β_4
1	$Bio = \beta_0 + \beta_1 \cdot DBH$	14.4	0.86	-2901.85	96.3	-	-	-
2	$Bio = \beta_1 \cdot NDVI\_2$	37.8	0.87	-	23168.7	-	-	-
3	$Bio = \beta_1 \cdot B1$	38.8	0.87	-	51.8	-	-	-
4	$Bio = \beta_1 \cdot (NDVI) + \beta_2 \cdot (SR) + \beta_3 \cdot (SAVI)$	39.6	0.86	-	549026	75.765	-36715	-
1	$Cb = \beta_0 + \beta_1 \cdot CA + \beta_2 \cdot DBH + \beta_3 \cdot h$	14.4	0.85	-1428.88	0.9038	41.249	6.161	-
2	$Cb = \beta_1 \cdot NDVI + \beta_2 \cdot NDVI\_1 + \beta_3 \cdot NDVI\_2 + \beta_4 \cdot NDVI\_3$	38.5	0.87	-	-27115.7	29405	33738.8	-25671.2
3	$Cb = \beta_0 + \beta_1 \cdot DBH$	14.3	0.86	-1260.91	42.0935	-	-	-
4	$Cb = \beta_1 \cdot NDVI$	38.5	0.87	-	1508.6	-	-	-
5	$Cb = \beta_1 \cdot NDVI\_2$	37.5	0.88	-	10194.4	-	-	-

Note. Bio = Biomass (kg); Cb = Carbon (kg); R. M. = Regression Model; Syx% = standard error of estimative; R^2adj = coefficient of determination adjusted; βi = parameters of the equation; h = total height (m); CA = Crown area.

For the models considering as dependent variable the carbon content (kg), the equations obtained some values close to those found with the biomass variable (kg). Equations 1 and 3 can be highlighted, being those that presented a smaller relative error in relation to the others. In Equation 3, a greater prominence is given by presenting values of 0.86 for the R^2 adj and 14.32% for the relative error. By the fact of they are independent variables directly related to individuals, that is, variables extracted from each tree in the field, such as the DBH and the crown area, it can be a point to be observed to justify the values presented in the equations Table 4.

For the equations with the vegetation indexes as independent variables, the values increased considerably, however, it is emphasized the Equation 2, which presents the three NDVIs modified in the research as independent variables, and that their values of R^2adj (0.87) and relative error (38.56%), did not show a significant difference with model 4, which uses the standard NDVI in the equation.

Ramirez et al. (2010) obtained a R^2adj of 0.85 and standard error of 5.1% for biomass, in which the independent variable was the green band of the satellite image Quickibird-2 for the coffee crop, contradicting this research in which the green band did not present satisfactory results to compare with the dependent variables, biomass and carbon.

The results are in accordance with the study by Watzlawick et al. (2009) to estimate biomass in an Araucaria Forest using the IKONOS-2 platform, using the NDVI, obtaining R^2adj of 0.53 and a standard error of 42.69%. Bendig et al. (2015), estimating the biomass of the summer barley crop in the Cologne municipality in Germany, where also using vegetation indexes for estimation, obtained R^2adj of 0.65 and a standard error of 56.45%. Both of the aforementioned studies obtained lower estimation results related to the present study.

The results of this study demonstrate the precision degree and importance of the Worldview-2 integration in the estimation of biomass and carbon. Dube and Mutanga (2015) obtained correlation coefficients from 0.86 to 0.92 for the estimation of biomass and carbon using vegetation indexes combined with spectral variables. These same authors commented that the humidity, slope, temperature, aspect, total moisture content, elevation and sunshine along with image spectral information significantly improved biomass and carbon estimates, because these factors influence vegetation growth and spectral response.

According to Watzlawick et al. (2009) the explanation about the near infrared presenting good results regarding biomass estimates it is closely associated with the vegetation, in the interaction of the incident energy with the cellular structure and the amount of water in the leaf. Dube and Mutanga (2015) commented that the use of vegetation indexes can be attributed to the saturation challenges associated with most multispectral sensors. The literature shows that NDVI calculated from traditional near-infrared and red bands produce poor biomass estimates (Hansen & Schjoerring, 2003; Lee et al., 2004; Mutanga & Skidmore, 2004). However, when compared with this study, NDVI-2 (near infrared and red-edge), obtained an acceptable result for biomass, mainly due to the Worldview-2 sensor characteristic.

For the graphical analysis of the residuals the best equations were chosen as a function of the R^2adj and the standard error, that can be visualized in Figure 5.

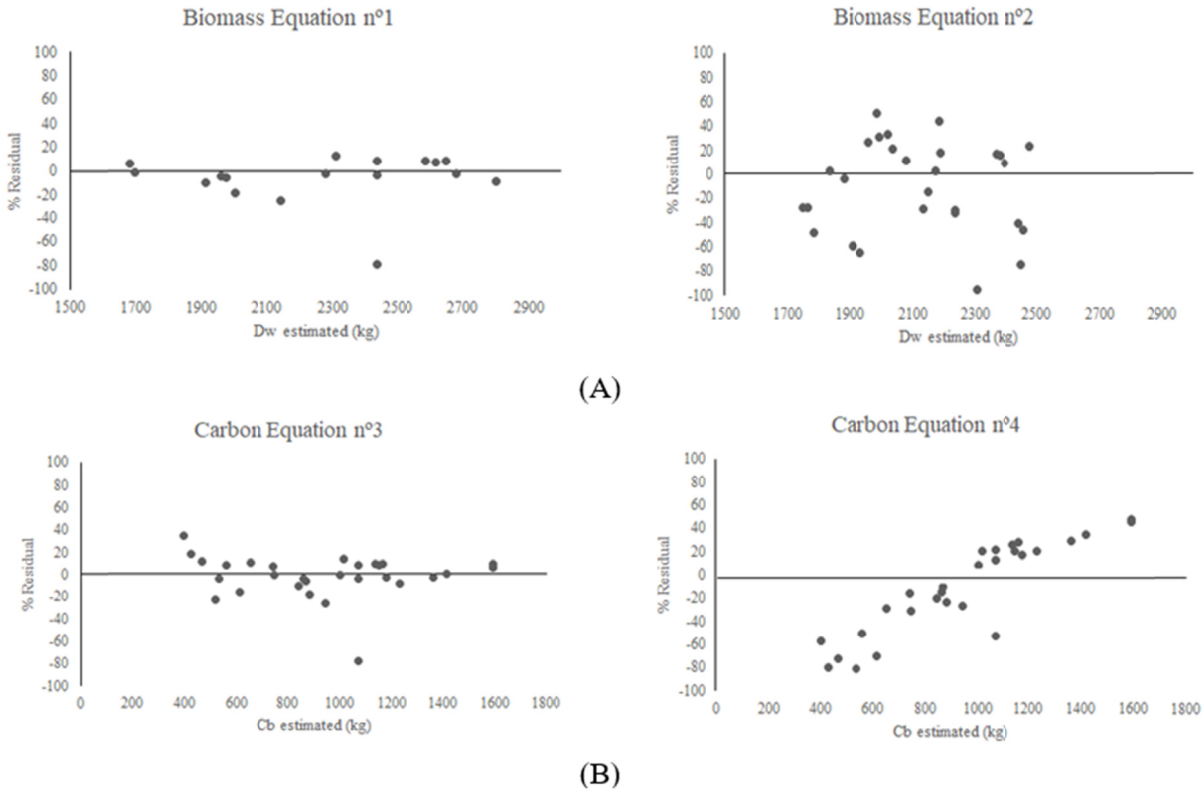

Figure 5. Residuals graphs for the best models for estimating biomass (A) and carbon (B) obtained by dendrometric and remote sensing variables

It can be observed that in the graphs shown in Figure 5 there were no trends in the distribution of residues. Highlighted it is presented the dendrometric variable DBH as independent for both biomass (Equation 1) and carbon (Equation 3), where its distribution is more uniform and distributed on the y-axis. The graphs with vegetation indexes as variable (Equation 2 for biomass and 4 for carbon) present more concentrated distributions, but without tendencies of overestimation or underestimation. This difference may be associated to the relationship between forest parameters and satellite spectral responses, which is still poorly understood in the scientific world, according to Lu et al. (2004).

Ferraz et al. (2012) estimating biomass in an area with semideciduous seasonal forest fragments and using image generated from the IKONOS II satellite, obtained similar results to those presented in Figure 5. The residuals graphs showing the spectral variables of the image, showed a graphical distribution close to those presented in graphs 1 and 3 of Figure 5, but the difference between the studies is that the independent variables of these graphs are dendrometric (DBH), confirming what was described previously in that these variables are more correlated with biomass.

4. Conclusion

This study investigated the potential of the multispectral sensor Worldview-2 using vegetation indexes in the estimation of biomass and carbon stocks in a fragment of Araucaria Forest in the southern region of the Parana State.

A high correlation between biomass and carbon can be observed in relation to the digital variables (spectral bands). The indexes that presented significant correlations were NDVI_2 and NDVI for biomass and carbon, respectively.

The results showed that the Worldview-2 high-resolution spatial sensor provides valuable primary data source for accurate and reliable estimation of biomass and carbon. The combined equations, especially with the NDVI, produced high estimates of R^2 adj, when compared to the traditional equation that considers only the variable DBH.

The methodology proposed in this study using the vegetation indexes was satisfactory, which makes the method advantageous, mainly in the sense of reducing the time spent in fieldwork related to estimates.

References

Adam, E., Mutanga, O., Abdel-Rahman, E. M., & Ismail, R. (2014). Estimating standing biomass in papyrus (*Cyperus papyrus* L.) swamp: Exploratory of in situ hyperspectral indices and random forest regression. *Int. J. Rem. Sens., 35*, 693-714. https://doi.org/10.1080/01431161.2013.870676

Anaya, J. A., Chuvieco, E., & Palacios-Orueta, A. (2009). Aboveground biomass assessment in Colombia: A remote sensing approach. *Forest Ecology and Management, 257*(4), 1237-1246. https://doi.org/10.1016/j.foreco.2008.11.016

Avitabile, V., Baccini, A., Friedl, M. A., & Schmullius, C. (2012). Capabilities and limitations of Landsat and land cover data for aboveground woody biomass estimation of Uganda. *Remote Sensing of Environment. 117*, 366-380. https://doi.org/10.1016/j.rse.2011.10.012

Becker D. R., Skog K., Hellman A., Halvorsen K. E., & Mace T. (2009). An outlook for sustainable forest bioenergy production in the Lake States. *Energy Policy, 37*(12), 5687-5693. https://doi.org/10.1016/j.enpol.2009.08.033

Bendig, J., Yu, K., Aasen, H., Bolten, A., Bennertz, S., Broscheit, J., Gnyp, M. L., & Bareth, G. (2015). Combining UAV-based plant height from crop surface models, visible, and near infrared vegetation indices for biomass monitoring in barley. *International Journal of Applied Earth Observation and Geoinformation, 39*, 79-87. https://doi.org/10.1016/j.jag.2015.02.012

Chuvieco, E. (1990). *Fundamentos de teledetección espacial* (p. 453). Ediciones Rialp, Madrid.

Clark, M. L., Roberts, D. A., Ewel, J. J., & Clark, D. B. (2011). Estimation of tropical rain forest aboveground biomass with small-footprint lidar and hyperspectral sensors. *Remote Sensing of Environment, 115*, 2931-2942. https://doi.org/10.1016/j.rse.2010.08.029

Cohen, W. B., & Spies, T. A. (1992). Estimating structural attributes of douglas-fir/western hemlock forest stands from Landsat and Spot imagery. *Remote Sensing of Environment, 41*, 1-17. https://doi.org/10.1016/0034-4257(92)90056-P

Da Silva, D. P., Poppiel, R. R., Baptista, G. M. M., & Moreira, E. C. G. (2017). Influência dos métodos de correção atmosférico FLAASH e QUAC na determinação do índice NDBSI de solos tropicais mediante dados hiperespectrais do sensor AVIRIS. *Simpósio Brasileiro de Sensoriamento Remoto, 18*, 2-9.

Dong, J. R., Kaufmann, R. K., Myneni, R. B., Tucker, C. J., Kauppi, P. E., Liski, J., … Hughes, M. K. (2003). Remote sensing estimates of boreal and temperate forest woody biomass: Carbon pools, sources, and sinks. *Remote Sensing of Environment, 84*, 393-410. https://doi.org/10.1016/S0034-4257(02)00130-X

Dube, T., & Mutanga, O. (2015). Evaluating the utility of the medium-spatial resolution Landsat 8 multispectral sensor in quantifying aboveground biomass in uMgeni catchment, South Africa. *ISPRS Journal of Photogrammetry and Remote Sensing, 101*, 36-46. https://doi.org/10.1016/j.isprsjprs.2014.11.001

Dube, T., Mutanga, O., Elhadi, A., & Ismail, R. (2014). Intra-and-inter species biomass prediction in a plantation forest: Testing the utility of high spatial resolution spaceborne multispectral Rapid Eye sensor and advanced machine learning algorithms Sensors. *Sensors (Basel), 14*(8), 15348-15370. https://doi.org/10.3390/s140815348

Fassnacht, F. E., Hartig, F., Latifi, H., Berge, C., Hernández, J., Corvalán, P., & Koch, B. (2014). Importance of sample size, data type and prediction method for remote sensing-based estimations of aboveground forest biomass. *Remote Sensing of Environment, 154*, 102-114. https://doi.org/10.1016/j.rse.2014.07.028

Fassnacht, F. F., Mangold, D., Schäfer, J., Immitzer, M., Kattenborn, T., Koch, B., & Latifi, H. (2017). Estimating stand density, biomass and tree species from very high resolution stereo-imagery—Towards an all-in-one sensor for forestry applications? *Forestry: An International Journal of Forest Research, 90*(5), 613-631. https://doi.org/10.1093/forestry/cpx014

Ferraz, A. S. (2012). *Estimação dos estoques de biomassa e carbono na parte aérea de um fragmento de floresta estacional Semidecidual por meio de imagens de satélite Ikonos II* (103f., Thesis, Doctor in Forest Science, Federal University of Viçosa, Brazil).

Gleason, C. J., & Im, J. (2011). A review of remote sensing of forest biomass and biofuel: Options for small-area applications. *GIsci. Remote Sens., 48*, 141-170. https://doi.org/10.2747/1548-1603.48.2.141

Gurgel, H. da C. (2003). *Variabilidade espacial e temporal do NDVI sobre o Brasil e suas conexões com o clima* (118f., Dissertation, Master in Remote Sensing, Instituto Nacional de Pesquisas Espaciais-INPE, Brazil).

Hansen, P. M., & Schjoerring, J. K. (2003). Reflectance measurement of canopy biomass and nitrogen status in wheat crops using normalized difference vegetation indices and partial least squares regression. *Remote Sensing of Environment, 86*(4), 542-553. https://doi.org/10.1016/S0034-4257(03)00131-7

Huete, A. R. A. (1988). Soil-Adjusted Vegetation Index (SAVI). *Remote Sensing of Environment, 25*(3), 295-309. https://doi.org/10.1016/0034-4257(88)90106-X

Koch, B. (2010). Status and future of laser scanning, synthetic aperture radar and hyperspectral remote sensing data for forest biomass assessment. *ISPRS Journal of Photogrammetry and Remote Sensing, 65*, 581-590. https://doi.org/10.1016/j.isprsjprs.2010.09.001

Lee, K. S., Cohen, W. B., Kennedy, R. E., Maiersperger, T. K., & Gower, S. T. (2004). Hyperspectral versus multispectral data for estimating leaf area index in four different biomes. *Remote Sensing of Environment, 91*(3-4), 508-520. https://doi.org/10.1016/j.rse.2004.04.010

Lu, D. (2006). The potential and challenge of remote sensing-based biomass estimation. *International Journal of Remote Sensing, 27*, 1297-1328. https://doi.org/10.1080/01431160500486732

Lu, D., & Batistella, M. (2005). Exploring TM image texture and its relationships with biomass estimation in Rondônia, Brazilian Amazon. *Acta Amazonica, 35*, 249-257. https://doi.org/10.1590/S0044-59672005000200015

Lu, D., Chen, Q., Wang, G., Moran, E., Batistella, M., Zhang, M., Laurin, G. V., & Saah, D. (2012). Aboveground forest biomass estimation with landsat and LiDAR data and uncertainty analysis of the estimates. *Int. J. Forestry Res.* https://doi.org/10.1155/2012/436537

Lu, D., Mausel, P., Brondizio, E., & Moran, E. (2004). Relationship between forest stand parameters and Landsat TM spectral responses Im the Brazilian Amazon Basin. *Forest Ecology and Management, 198*(1-3), 149-167. https://doi.org/10.1016/j.foreco.2004.03.048

Maack, J., Kattenborn, T., Fassnacht, F. E., Enßle, F., Hernández, J., Corvalán, P., & Koch, B. (2015). Modeling forest biomass using Very-High-Resolution data—Combining textural, spectral and photogrammetric predictors derived from spaceborne stereo images. *European Journal of Remote Sensing, 48*, 245-261. https://doi.org/10.5721/EuJRS20154814

Mutanga, O., & Skidmore, A. K. (2004). Narrow band vegetation indices overcome the saturation problem in biomass estimation. *Int. J. Rem. Sens., 25*, 3999-4014. https://doi.org/10.1080/01431160310001654923

Mutanga, O., Adam, E., & Cho, M. A. (2012). High density biomass estimation for wetland vegetation using WorldView-2 imagery and random forest regression algorithm. *Int. J. Appl. Earth Obs. Geoinf., 18*, 399-406. https://doi.org/10.1016/j.jag.2012.03.012

Ozdemir, I., & Karnieli, A. (2011). Predicting forest structural parameters using the image texture derived from WorldView-2 multispectral imagery in a dryland forest, Israel. *Int. J. Appl. Earth Obs. Geoinf, 13*, 701-710. https://doi.org/10.1016/j.jag.2011.05.006

Popescu, S. C., Wynne, R. H., & Scrivani, J. A. (2004). Fusion of small-footprint lidar and multispectral data to estimate plot-level volume and biomass in deciduous and pine forests in Virginia, USA. *Forest Sci., 50*, 551-565.

Ramirez, G. M., & Zullo Júnior, J. (2010). Estimativa de parâmetros biofísicos de plantios de café a partir de imagens orbitais de alta resolução espacial. *Engenharia Agrícola, 30*(3), 468-479. https://doi.org/10.1590/S0100-69162010000300011

Robinson, T. P., Wardell-Johnson, G. W., Pracilio, G., Brown, C., Corner, R., & Van Klinken R. D. (2016). Testing the discrimination and detection limits of WorldView-2 imagery on a challenging invasive plant target. *Int. J. Appl. Earth Obs., 44*, 23-30. https://doi.org/10.1016/j.jag.2015.07.004

Roik, M. (2018). *Biomassa aérea e carbono orgânico em árvores nativas de Araucaria angustifolia (Bertol.) Kuntze* (148f., Thesis, Doctor in Forest Engineering, Federal University of Parana, Brazil).

Sarker, L. R., & Nichol, J. E. (2011). Improved forest biomass estimates using ALOS AVNIR-2 texture indices. *Remote Sensing of Environment, 115*, 968-977. https://doi.org/10.1016/j.rse.2010.11.010

Schlerf, M., Atzberger, C., & Hill, J. (2005) Remote sensing of forest biophysical variables using HyMap imaging spectrometer data. *Remote Sensing of Environment, 95*(2), 177-194. https://doi.org/10.1016/j.rse.2004.12.016

Sibanda, M., Mutanga, O., & Rouget, M. (2015). Examining the potential of Sentinel-2 MSI spectral resolution in quantifying above ground biomass across different fertilizer treatments. *ISPRS Journal of Photogrammetry and Remote Sensing, 110*, 55-65. https://doi.org/10.1016/j.isprsjprs.2015.10.005

Soenen, S. A., Peddle, D. R., Hall, R. J., Coburn, C. A., & Hall, F. G. (2010). Estimating aboveground forest biomass from canopy reflectance model inversion in mountainous terrain. *Remote Sensing of Environment, 114*, 1325-1337. https://doi.org/10.1016/j.rse.2009.12.012

Tan, Q., Shao, Y., Yang, S., & Wei, Q. (2003) Wetland Vegetation Biomass Estimation Using Landsat-7 ETM+ Data. *IEEE Transactions on Geoscience and Remote Sensing, 3*, 2629-2631.

Tsui, O. W., Coops, N. C., Wulder, M. A., Marshall, P. L., & Mccardle, A. (2012). Using multifrequency radar and discrete-return LiDAR measurements to estimate aboveground biomass and biomass components in a coastal temperate forest. *Isprs J. Photogrammetry Remote Sens., 69*, 121-133. https://doi.org/10.1016/j.isprsjprs.2012.02.009

Watzlawick, L. F., Kirchner, F. F., & Sanquetta, C. R. (2009). Estimativa de biomassa e carbono em floresta com araucária utilizando imagens do satélite Ikonos II. *Ciência Florestal, 19*(2), 169-181. https://doi.org/10.5902/19805098408

Wrege, M. S., Steinmetz, S., Reisser Júnior, C., & De Almeida, I. R. (2012). *Atlas climático da região sul do Brasil: Estados do Paraná, Santa Catarina e Rio Grande do Sul* (p. 334). Pelotas: Embrapa Clima Temperado.

Xiaolin, Z., & Desheng, L. (2015). Improving forest aboveground biomass estimation using seasonal Landsat NDVI time-series. *ISPRS Journal of Photogrammetry and Remote Sensing, 102*, 222-231. https://doi.org/10.1016/j.isprsjprs.2014.08.014